Exceptionally Stable Dimers and Trimers of Au 25 Clusters Linked with a Bidentate Dithiol: Synthesis, Structure and Chirality Study

Michal Swierczewski, Fabrice Cousin, Ewa A Banach, Arnulf Rosspeintner, Latevi Max Lawson Daku, Abolfazl Ziarati, Rania Kazan, Gunnar Jeschke, Raymond Azoulay, Lay-theng Lee, et al.

Gold Clusters

How to cite:
International Edition: doi.org/10.1002/anie.202215746
German Edition: doi.org/10.1002/ange.202215746

Exceptionally Stable Dimers and Trimers of Au_{25} Clusters Linked with a Bidentate Dithiol: Synthesis, Structure and Chirality Study

Michal Swierczewski, Fabrice Cousin, Ewa Banach, Arnulf Rosspeintner, Latevi Max Lawson Daku, Abolfazl Ziarati, Rania Kazan, Gunnar Jeschke, Raymond Azoulay, Lay-Theng Lee, and Thomas Bürgi**

Abstract: A bidentate chiral dithiol (diBINAS) is utilised to bridge Au_{25} nanoclusters to form oligomers. Separation by size allows the isolation of fractions that are stable thanks to the bidentate nature of the linker. The structure of the products is elucidated by small-angle X-ray scattering and calculated using density functional theory. Additional structural details are studied by diffusion-ordered nuclear magnetic resonance spectroscopy, transmission electron microscopy and matrix-assisted laser desorption/ionization time of flight mass spectrometry. Significant changes in the optical properties are analysed by UV/Vis and fluorescence spectroscopies, with the latter demonstrating a strong emission enhancement. Furthermore, the emergent chiral characteristics are studied by circular dichroism. Due to the geometry constraints of the nanocluster assemblies, diBINAS can be regarded as a templating molecule, taking a step towards the directed self-assembly of metal clusters.

Introduction

Self-assembly of nanoparticles into superstructures with controlled morphologies presents an innovative pathway for the fabrication of novel materials through the emergence of distinct properties as well as the enhancement of the existing optical[1] and electronic effects[2] via their collective action. Hence, an opportunity is exposed to expand the plethora of applications of nanoparticles spanning from sensing[3] and electronics[2a,4] to photocatalysis[5] and biology.[6]

Typically, self-assembly is associated with attaining a thermodynamic equilibrium, whereby the superstructure resides at the minimum free energy of the system. Through careful selection of the building blocks and the application of a directing agent or a template, the spontaneous organisation of nanoparticles into ordered superstructures can be facilitated. Such a process is known as directed self-assembly and offers the advantage of not being limited to the global free energy minimum: complex spatial configuration can freeze the structure in a low entropy state constituting a local minimum on the free energy surface.[7]

Monolayer-protected nanoclusters are the perfect candidates for the study of self-assembly processes owing to their unusual stability, monodispersity and unique size-dependent optical properties. Hence, they offer promising characteristics when expanded to superstructures.[8] Particular attention of the ongoing research revolves around the assembly of thiolate-protected gold clusters, chiefly explained by the strength of the covalent Au–S bond. Therefore, the prevalent strategy employs dithiol ligands as a bridge between two or more building blocks,[9] though examples of thiol-free linking are also known.[10]

A common pervasive drawback of assembling gold nanocluster oligomers and multimers is the dynamic nature of the system, which poses consequential analytical challenges: separation of the products by size prior to the analysis is futile if they continue reacting and forming new species. In fact, it has been shown that thiolates can exchange between clusters even in the absence of free thiols in solution.[11]

Here, we address this issue by introducing a new dithiol ligand, which binds in a bidentate fashion: (1*R*,1′*R*)-6,6′-(1,4-phenylene)di-1,1′-binaphthyl-2,2′-dithiol or diBINAS (see Figure 1). Previous ligand exchange reactions between the monomeric bidentate ligand, 1,1′-binaphthyl-2,2′-dithiol (or BINAS) and $Au_{25}PET_{18}$ (PET = phenylethanethiol, SC_2H_4Ph) exhibited a slower reaction rate than typically observed when using monodentate thiolates. However, the resulting products tended to be less dynamic and reluctant to proceed with the reverse reaction.[12] Additionally,

[*] M. Swierczewski, Dr. E. Banach, Dr. A. Rosspeintner, Dr. L. M. Lawson Daku, Dr. A. Ziarati, Dr. R. Kazan, R. Azoulay, Prof. T. Bürgi
Department of Physical Chemistry, University of Geneva
30 Quai Ernest-Ansermet, 1211 Geneva 4 (Switzerland)
E-mail: Thomas.Buergi@unige.ch

Dr. F. Cousin, Dr. L.-T. Lee
Laboratoire Léon Brillouin, Université Paris-Saclay
CEA-Saclay, 91191 Gif-sur-Yvette Cedex (France)
E-mail: Lay-Theng.Lee@cea.fr

Prof. G. Jeschke
Department of Chemistry and Applied Biosciences, ETH Zürich
Vladimir-Prelog-Weg 1–5/10, 8093 Zürich (Switzerland)

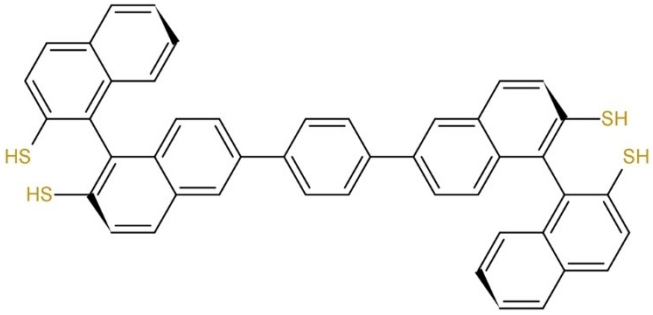

Figure 1. (1*R*,1′*R*)-6,6′-(1,4-phenylene)di-1,1′-binaphthyl-2,2′-dithiol.

numerous studies backed by density functional theory (DFT) calculations identified the preferred binding site on the $Au_{25}(SR)_{18}$ cluster.[12a,13] In fact, the distance between two S atoms in the BINAS molecule perfectly matches with the interstaple binding mode. Given the heavy geometrical constraints directing the bridging of $Au_{25}PET_{18}$ building blocks, we think of diBINAS as a templating molecule, taking an important step towards the directed self-assembly of metal clusters,[7a,14] which is yet to be achieved for nanoparticles in such a small size regime (below 2 nm).

The products of the linking reaction between $Au_{25}PET_{18}$ and diBINAS are subjected to size-exclusion chromatography (SEC) and studied in detail using small-angle X-ray scattering (SAXS), where we focus primarily on the dimers and the trimers to confirm the successful reduction in the dynamism of the system. The emergent chiral properties are measured with circular dichroism (CD). Complementary analytical techniques include UV/Vis and fluorescence spectroscopies, matrix-assisted laser desorption/ionisation time of flight mass spectrometry (MALDI-TOF MS), diffusion-ordered nuclear magnetic resonance spectroscopy (DOSY NMR), electron paramagnetic resonance (EPR) and transmission electron microscopy (TEM).

We think that the most prominent advantage of our linker ligand over those used in similar oligomer systems is the strength of the bidentate bonding resulting in a substantial increase in the stability and reduction in the dynamism of the linked molecules, which greatly facilitates the efficient analysis of well isolated fractions. This additional degree of control over the monodispersity and the binding mode of the assemblies is crucial in the advancement of the family of conjugated cluster oligomers for their prospective applications in molecular electronics and the study of electron transfer dynamics.[9b]

Results and Discussion

The Au_{25} monomers were linked using a tailor-designed bifunctional thiol molecule. The details of the multi-step synthetic route leading to diBINAS are included in Figures S1 and S2. The main criteria considered in order to contrive the molecule were: (i) bidentate bonding of the ligand which, while reducing the rate of oligomerisation initially, also drastically decreases the lability of the bridging ligand once the connection is established; (ii) high bridge rigidity to eliminate the possibility of intracluster binding; (iii) considerable separation between binding points on the ligand to reduce steric hindrance when the reacting cluster molecules approach each other; (iv) chirality to study the emergent properties and their changes from the free ligand to the bound state.

Although generally the cluster to linker ratio that most efficiently promotes dimer formation is 2:1,[9b] diBINAS exhibits a much slower binding rate than typical monodentate bridges, which suggests that the proportion of the thiol should be increased.[12a] Following separation by size on a SEC column, we found the cluster to thiol ratio of 1:3 to be optimal for forming oligomers, which are the focus of our analysis; insufficient thiol resulted in little Au_{25} undergoing exchange, while too much of the ligand favoured the formation of larger multimers.

Large multimers that eluted first were found to show no distinct peaks in the 1.6–3.1 eV range of the UV/Vis absorption spectra, while the concentrated band that eluted last was found to be unreacted $Au_{25}PET_{18}$. The middle fraction of the SEC column showed major changes in the absorption spectrum, and therefore, this is where we focus our analysis by SAXS. From SAXS (see following section) the UV spectra that correspond to the dimer, the trimer and the tetramer fractions were identified, as seen in Figure 2. Henceforth, these will be used as the point of reference for other measurements and together commonly referred to as the oligomer fractions.

The UV/Vis absorption spectrum of the monomeric $Au_{25}PET_{18}$ can be characterised by three distinct peaks: at 1.8, 2.8 and 3.1 eV.[15] These well-defined features can be observed thanks to the atomically precise structure and are known to be commonly exhibited by gold nanoclusters. However, when the oligomers are formed, these peaks in the 1.6–3.1 eV range are gradually flattened as a result of

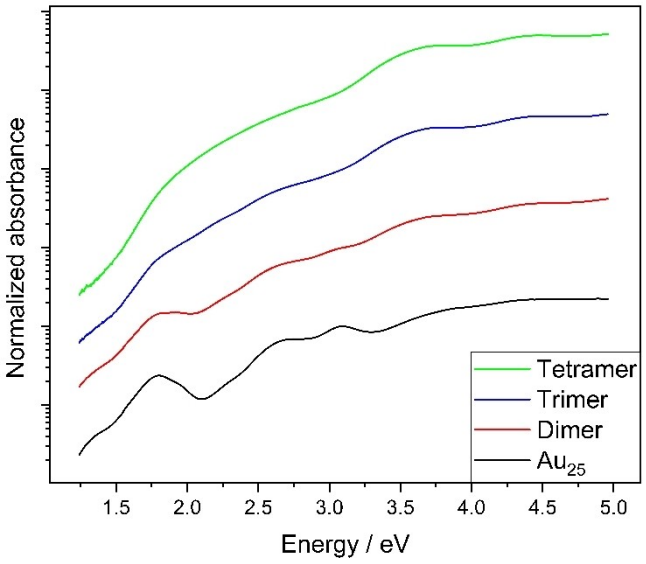

Figure 2. UV/Vis spectra of the fractions with the sizes assigned by SAXS (normalised at 3.1 eV, logarithmically offset for clarity).

the reduction of symmetry of the cluster: as the size of the oligomer increases, the number of possible structural isomers as well as that of allowed conformers increases, resulting in small shifts of the absorption spectrum and hence, in the broadening of the features. The geometry of such a structural isomer of the dimer has been optimised within DFT (see Supporting Information for the structures and calculation details). The absorption spectrum based on one of these geometries has been simulated and is shown in Figure S3. Although a reasonable match is observed between the experimental and the calculated spectra for the dimer, the visible discrepancies exemplify the complexity of the system.

The changes in UV absorption spectra above 3.1 eV are dominated by ligand absorption and are discussed in Figure S4.

SAXS is a widely applied method for the study of structural information such as the size and the shape of nanosized particles in solution.[16] The technique is based on the electronic scattering length density, meaning that the scattering signal originates mainly from the electron-rich gold core and the staples. Consequently, the contribution of the organic shell and the dithiol linker is relatively insignificant and the size derived from SAXS reflects that of the Au core and is expected to be smaller than the value obtained for the crystal structure of a thiol-protected cluster.[15b,17]

The scattering intensities, I(Q), normalised by the concentration are plotted as a function of the scattering vector, $Q = 4\pi sin(\theta)/\lambda$, in Figure 3(a) for different isolated fractions. The scattering intensity increases with the order of elution from smaller to larger oligomer and the Guinier plateau in the scattering curves indicates that each fraction is characterised by a well-defined size accessible within the Q-range of the measurement. Qualitatively, since the limiting scattering intensity $I(Q)(Q\rightarrow 0)$ is proportional to the volume of the scattering object, the ratio of this limiting intensity for an oligomer and the monomer gives a good indication of the relative size of the oligomer, as defined by N in the equation below:

$$N = \frac{I(Q)_{Q\rightarrow 0}[(Au_{25}(PET)_{16})_2(Au_{25}(PET)_{14})_{(x-1)}(diBINAS)_x]}{I(Q)_{Q\rightarrow 0}[Au_{25}(PET)_{18}]} \quad (1)$$

where $Au_{25}(PET)_{16}$ and $Au_{25}(PET)_{14}$ refer to terminal and non-terminal pearls respectively. For the isolated fractions of smaller oligomers shown in Figure 3(a), N is found to increase in regular increments from 1 for the unlinked monomer to about 3 for the linked oligomers.

The scattering curve for the unlinked $Au_{25}PET_{18}$ was fitted using a non-interacting hard-sphere model, yielding a radius of 4.6 Å, which is in perfect agreement with the value obtained in the past for $Au_{25}(SBut)_{18}$ by our group.[9b] For the linked oligomers with N close to an integer, a pearl necklace model based on hard spheres joined by rigid strings was found to best characterise the system. Excellent fits were obtained for the fractions with $N \approx 2.1$ and $N \approx 3.0$ using a 2-pearl (dimer) and a 3-pearl (trimer) model respectively. The fits yield Au core radius $R = 4.6$ and 4.7 Å and edge-edge distance (separation between pearls) $L = 12.8$ and 13.7 Å for the dimer and the trimer respectively. These results are shown together with the unlinked monomer in Figure 3(b). The fractions with $N \approx 1.2$–1.8 indicate mixtures and a mixed model of volume fraction x[hard sphere

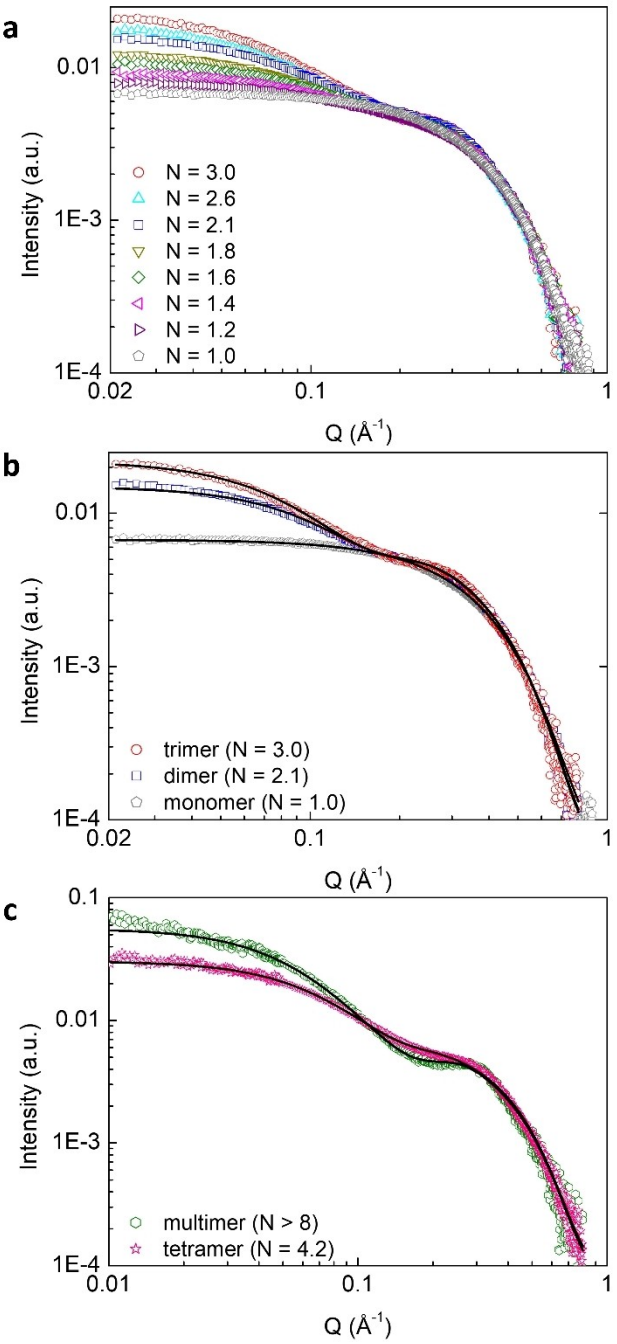

Figure 3. (a) SAXS curves of fractions separated by SEC; N is the relative scattering intensity with respect to the monomer intensity at $\lim(Q\rightarrow 0)$ as defined in the main text, (b) unlinked monomer and linked oligomers $N \approx 2.1$ and $N \approx 3.0$ fitted with hard sphere model and with 2-pearl (dimer) and 3-pearl (trimer) necklace model respectively (solid lines), (c) multimers $N \approx 4.2$ and $N > 8$ fitted with 4-pearl (tetramer) and 8-pearl (octamer) necklace model respectively (solid lines). The fitted values are given in Table 1.

monomer] and $(1-x)$[pearl necklace dimer] gives very good fits. Similarly, the fraction $N\approx2.6$ can be described well by a mixed model comprised of dimers and trimers based on the pearl necklace model. Although these mixed fractions are not the focus of this study, it was found that the ratios of the scaling factors of each component agree very well with the value of N (see Figure S5).

Larger linked structures were also isolated, for which the measurement was extended to lower Q (see Figure 3(c)). These larger oligomers, $N\approx4.2$ and $N>8$ are fitted with 4-pearl and 8-pearl model and referred to as the tetramer and the multimer respectively. The fitted results yield $R=4.7$ Å and $L=13.7$ Å for the tetramer, and $R=4.6$ Å and $L=13.9$ Å for the multimer. Thus overall, the linked systems appear to maintain the integrity of the Au core with $R=4.6$–4.7 Å and cluster edge-edge separation $L=12.8$–13.9 Å. Note the small but visible structure peak at $Q\approx0.28$–0.30 Å which gives a corresponding Au core-core distance ≈20–22 Å, in good agreement with the fitted edge-edge distance. Importantly, this structure peak does not vary in position but increases in intensity with oligomer size as the number of linked clusters increases. This observation reinforces our model of pearl necklace structure of linked Au clusters separated by a well-defined distance. The fitted results are summarised in Table 1.

It is interesting to compare the large multimer fraction ($N>8$) linked by the bidentate diBINAS with the monodentate linker p-terphenyl-4,4″-dithiol used in a previous study by our group.[9b] In the case of the monodentate ligand, the multimer showed a significant small-angle rise that could not be fitted with the pearl necklace model but was well-described by a sticky sphere model where multiple links between gold cores are possible, forming a dense aggregate network. On the contrary, the multimer based on diBINAS maintains an open structure of a connected chain. This is consistent with diBINAS being much more selective to its binding position, which is constrained by the geometry of the cluster and the preference for interstaple binding, as discussed in the introduction, hence obstructing network formation. It is crucial to emphasise that no small-angle rise is observed in any of the diBINAS-linked samples, attesting to the absence of large aggregates such as those formed by monodentate linkers. The low degree of dynamism can be attributed to the strong chelating Au–S bond formed by the bidentate ligand linker, thus limiting the further reaction of the already formed products.

NMR DOSY spectroscopy is a good complimentary method to SAXS because it is particularly effective at calculating the hydrodynamic radius, r_H, of multimer fractions, for which we could not define the absolute size by SAXS due to their Guinier plateau falling outside of the Q-range accessible with the experimental configuration used. Conversely, DOSY is less efficient at calculating r_H of smaller oligomers, particularly if their shape is not spherical, which is the case for oligomer fractions considered here. Therefore, in our analysis we grant higher confidence to SAXS measurements for the oligomers and to DOSY for the multimers.

The modified Stokes-Einstein equation was used to determine r_H using the value of the diffusion coefficient, D_t, obtained from NMR experiments:

$$r_H = \frac{k_B T}{6 f_s(a,b)\pi\eta D_t} \quad (2)$$

where k_B is the Boltzmann constant, T is the temperature, f_s is the correcting factor for non-spherical molecules according to Perrin's equations for prolate molecules,[18] and η is the viscosity of the solvent.

The shape factor f_S depends on the ratio a/b between the major (a) and minor (b) semiaxes of the ellipsoid and is applied here for the calculation of r_H of the dimer, for which the geometry is well-defined and constrained by the linker ligand. Applying the dimensions for the semiaxes obtained from SAXS to the Perrin's equations yields a correcting factor of 1.14 that is used for the dimer molecule (calculation included in Supporting Information). For all other sizes of molecules studied here the exact geometry is not well-defined so the standard Stokes–Einstein equation is employed, i.e. $f_s=1$.

The DOSY spectra of the oligomers and the multimer fractions are included in the Figure S6. The average D_t values obtained from three different regions of the NMR spectra and the calculated r_H are given in Table 2. For the dimer, the trimer and the tetramer fractions the calculated r_H were 0.93, 1.00 and 1.03 nm respectively. As a point of reference, Salorinne and co-workers reported a value of 0.84 nm for monomeric $Au_{25}PET_{18}$,[19] bordering on the value of 0.88 nm obtained by our group for $Au_{25}(SBut)_{18}$.[9b] For the multimer fraction r_H was calculated to be 2.33 nm, which gives the effective volume of 21.4 times that of the monomer. It should be noted that the diffusing multimers

Table 1: Summary of the fitted SAXS results. The hardsphere model was used for the monomer and the pearl necklace model for all other fractions. The polydispersity of radius R was fixed at 0.20 in all cases.

Fraction	R [Å]	No. pearls	Edge-edge distance [Å]
Monomer	4.55	–	–
Dimer	4.66	2	12.81 ± 0.50
Trimer	4.63	3	13.66 ± 0.57
Tetramer	4.67	4	13.65 ± 0.79
Multimer	4.63	8	13.94 ± 0.45

Table 2: Summary of DOSY NMR results. D_t is an average of values in the aromatic region, the 5.30–5.01 ppm region and the 4.0–2.5 ppm region; individual values are given in Figure S6; f_s is the non-spherical shape factor calculated according to Perrin's equations; r_H is the calculated hydrodynamic radius and V_{Au25} is the factor by which the effective volume of the multimer is larger than that of the monomer.

Fraction	Average D_t [$m^2 s^{-1}$]	f_s	r_H [nm]	V_{Au25}
Dimer	5094	1.14	0.91	1.3×
Trimer	5265	1	1.00	1.7×
Tetramer	5134	1	1.03	1.8×
Multimer	2309	1	2.33	21.4×

also contain solvent molecules trapped between the linked clusters so the real number of monomer units constituting a multimer is considerably less than 21.4.

MALDI-TOF MS spectra (Figure 4) were recorded for the linked systems with different values of N based on the SAXS measurements. The peaks at 7391 and 6055 *m/z* are characteristic of $Au_{25}PET_{18}$ with the former being the molecular ion peak and the latter resulting from a loss of Au_4PET_4 fragment. Both peaks gradually decrease in relative intensity as *N* increases, indicating that the contribution of the monomer in the mixture declines. As evidenced from CD measurements (see following section), it is highly unlikely for a diBINAS ligand to bind to one cluster without bridging to another one. Moreover, such species were not found in our previous work with monodentate linker ligands.[9b] Therefore, in this case, the exchange cannot be followed by a simple difference in ligands' molecular weight. Instead, the calculated masses of the dimer and trimer fractions (14945 and 22773 Da respectively) necessitate the formation of doubly or triply charged species in order to be detectable in the range of the measurement. Coupled with a high degree of fragmentation expected for the linked systems, their molecular ion peaks predicted at 7473 and 7591 *m/z* were not found.

Instead, peaks corresponding to either the dimer or the trimer fractions respectively could be identified simply by comparing their relative intensities between fractions of different N. For instance, peaks at 6455 and 7792 *m/z* (labelled in red in Figure 4) exhibit a particular prominence in fractions rich in the dimer ($N=1.8$, 2.1, 2.6) but their relative intensity gradually decreases when $N=3$–4. Moreover, peaks at 7115, 7517, 7671 and 8195 *m/z* (labelled in green in Figure 4) along with the envelope of peaks in the range of 6400–7100 *m/z*, could be assigned exclusively to trimers, as they emerge when $N>2.6$. In other words, peaks characteristic of the terminal pearl (based on the singly exchanged -$Au_{25}PET_{16}$- unit) dominate the dimer spectra

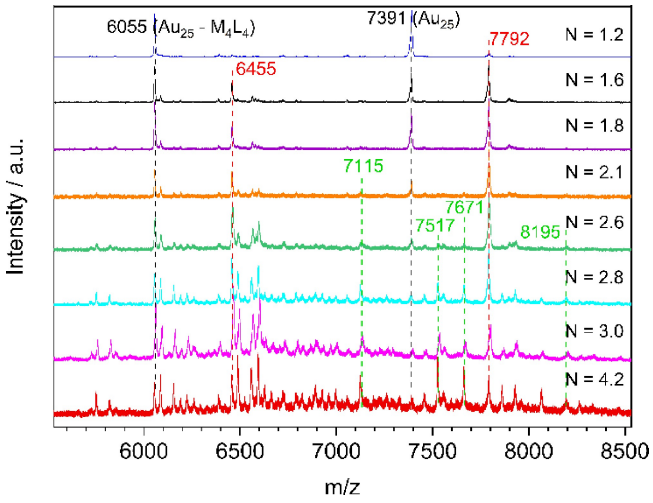

Figure 4. MALDI-TOF MS spectra of different fractions, offset for clarity. Peaks characteristic for the dimer and the trimer are shown in red and green respectively. Assigned structures are shown in Table 3.

while the relative proportion of peaks signifying a central pearl (doubly exchanged -$Au_{25}PET_{14}$- unit) gradually increase with increasing N. Possible structures for all of these peaks have been proposed in Table 3.

In this table, the purported formation mechanism of the different structures considers that the diBINAS molecule remains attached to $Au_{25}PET_{18-2x}$ from one side but breaks its chelating Au–S bond on its opposite side and additionally loses an -SH group. The most possible configuration that the structures could attain is a thiophene-like sulphur bridge linking two adjacent naphthalene groups. This functional group was isolated as a side-product formed at 280 °C along the synthetic pathway of diBINAS (see Figure S7 for details). Seeing how the step leading to the formation of the thiophene required a high temperature, observing similar behaviour under the influence of a laser might not be surprising.

Since $Au_{25}PET_{18}$ is achiral but diBINAS is chiral, CD measurements provide a direct proof of incorporation of the ligand and offer the opportunity to study the emergent chirality of differently sized oligomers. The anisotropy factors of the oligomers are presented in Figure 5. The corresponding ellipticity spectra are shown in Figure S8.

As expected, higher N values in all cases result in stronger anisotropy factors at a given wavelength. This suggests that bonding of diBINAS to one cluster through

Table 3: Proposed structures for selected MALDI-TOF MS peaks. Sulphur atoms are shown in green; (+2) corresponds to doubly charged species; $M_4L_4=Au_4PET_4$. The key part is the linker's S atom located away from the cluster, i.e. cleavage point from the complementary fragment (see main text).

m/z	Structure
Dimer	
7792	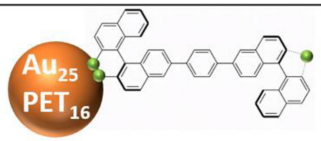
6455	7792-M_4L_4
Trimer	
8195	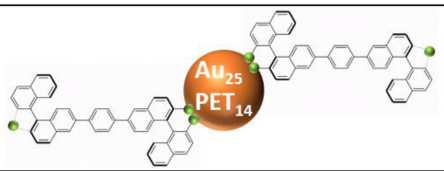
7671 (+2)	
7517	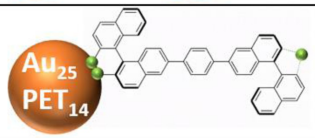
7115	$Au_{25}PET_{16}$

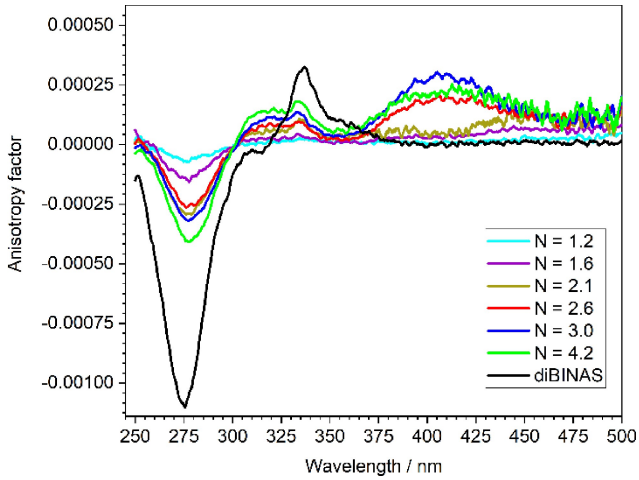

Figure 5. Anisotropy factors obtained from CD and UV/Vis spectra of different fractions. Due to negligible absorbance of diBINAS above 400 nm, its ellipticity is shown here as a reference.

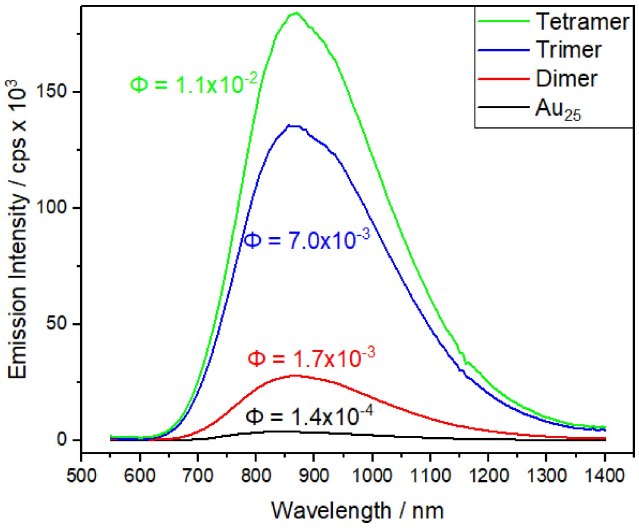

Figure 6. Fluorescence spectra of the fractions excited at 370 nm with the calculated quantum yields (Φ) included next to the relevant curves.

the chelating moiety without bridging it to another cluster is negligible—otherwise fractions with low N value should result in highest CD signals as they are able to accommodate more chiral ligands per cluster than the oligomers. In actuality, increasing oligomer size leads to higher ratio of diBINAS linkers to $Au_{25}PET_{18-2x}$ building blocks, hence intensifying the optical response.

Some optical features are common in all CD spectra, albeit small shifts are observed between the free and the bound ligand, such as the strong peak at 275 nm (red-shifted by 3 nm in the oligomers) and 337 nm (blue-shifted by 4 nm when bound). However, there are also peaks that appear only in the linked system such as the broad shoulder between 300–330 nm. Moreover, an intense positive response is observed at 410 nm and, interestingly, it is only manifested in multimers with $N>2.6$, indicating that this feature is characteristic of trimers and/or larger species. Further studies involving DFT calculations are needed to elucidate the possible origin of the formation of this feature. Nevertheless, it can be speculated that with the limited number of interstaple binding points that are accessible to diBINAS,[12a,b] simultaneous accommodation of two diBINAS molecules on the same -$Au_{25}PET_{14}$- moiety (central building block in the trimer) forces additional constraints, which might lead to a twisted configuration, and hence, a newly emergent chiral feature. This geometrical constraint is the reason why, based on SAXS, we do not see aggregates that have multipoint linkage.

Additionally, the fact that the CD spectra of the fractions with $N<2.1$ are completely flat in the region between 370–420 nm implies that the percentage of larger species that are chirally active at this wavelength is negligible, which again evidences the high degree of monodispersity and low dynamism of the separated oligomers.

The emission spectra of the monomer and the linked systems following excitation at 370 nm are shown in Figure 6. The quantum yields (Φ) at this excitation wavelength have been calculated by comparison with the quantum yield of Rhodamine 6G in MeOH. The relevant equation used is shown in the experimental part of the Supporting Information.[20] A significant enhancement of the broad fluorescence emission peak centred at 880 nm is observed with the increasing size of the linked system. Note that BINAS emits at around 400 nm. The quantum yields increase with respect to the monomer by a factor of 12 for the dimer, 49 for the trimer and 75 for the tetramer. This change can be attributed to the increased rigidity within the ligand shell of each cluster due to the restriction of intramolecular rotation induced by the bidentate bonding.[21] Higher rigidity leads to the diminished contribution of non-radiative pathways (k_{nonrad}) associated with free rotation, and hence, results in an increase in the contribution of the radiative pathways (k_{rad}). This conclusion is further confirmed by studying the fluorescence of monomeric $Au_{25}PET_{(18-2x)}(R\text{-BINAS})_x$: when $\bar{x}\approx 2.5$–3, the quantum yield increases with respect to that of $Au_{25}PET_{18}$ by a factor of 28 (Figure S9).

Fluorescence details have been further studied with the use of time-correlated single-photon counting (TCSPC), the results of which are plotted in Figure S10. The experimental data was successfully fitted using a Kohlrausch stretched exponential model presented in the following equation:[22]

$$\Phi(t) = A\exp\left[-\left(\frac{t}{\pi}\right)^{\beta}\right] \quad (3)$$

where β is an empirical exponent and τ is the lifetime. The fitted parameters for TCSPC spectra for the dimer, the trimer and the tetramer fraction are shown in a table attached to Figure S10. The distributions are similarly asymmetric for all samples ((β) is within 0.44–0.48 in all cases) but τ increases monotonously with the sample complexity, with $\tau=68$, 106 and 135 ns for the dimer, the trimer and the tetramer respectively.

Given that Φ of the gold clusters considered here are very low, it can be assumed that $k_{rad} \ll k_{nonrad}$. It, therefore, follows that the relationships $\Phi = k_{rad}/(k_{rad}+k_{nonrad})$ and $\tau = 1/(k_{rad}+k_{nonrad})$ can be approximated by $\Phi \approx k_{rad}/k_{nonrad}$ and $\tau \approx 1/k_{nonrad}$ respectively.

The first relationship does not clarify whether k_{rad} increases or if k_{nonrad} decreases as Φ increase for larger oligomers. However, from the second relationship, it is evident that as τ increases with the sample complexity, it is the contribution of the non-radiative pathways that has to decrease, consistent with the increasing rigidity of the ligand shell of the linked clusters discussed before.

Since the monomeric $Au_{25}PET_{18}$ cluster is a radical, the dimer should be treated as a biradical exhibiting a singlet or a triplet electronic ground state. A singlet ground state would then point towards an operative electronic coupling between the gold clusters mediated by the bridging ligand. However, the absence of any significant differences between the normalised emission spectra of $Au_{25}PET_{(18-2x)}$(*R*-BINAS)$_x$ and the larger oligomers (Figure S9) suggests that such a coupling between the clusters is negligible. This result is consistent with the DFT calculations of the energy difference between the singlet and the triplet state of the dimer ($\Delta E_{ST} = -604\ cm^{-1}$, see Supporting Information for calculation details), which implies a triplet ground state lying slightly below the singlet state and which thus suggests a weak to vanishing electronic coupling between the linked Au_{25} clusters.

Further evidence for negligible electronic coupling was obtained experimentally by electron paramagnetic resonance (EPR) measurements, whereby both normal EPR and Hyperfine Sub-level Correlation (HYSCORE) spectra are almost identical for monomeric $Au_{25}PET_{18}$ and the dimer (see Figure S11).

TEM was used to image the oligomers, as seen in Figure 7. The length of the Au_{25}-linker-Au_{25} units was measured to be 3.28 ± 0.37 nm in the dimer and 3.15 ± 0.35 nm in the trimer, which is in good agreement with the dimensions calculated based on the fitted SAXS curves (3.15 nm and 3.22 nm respectively). It should be noted that since a trimer molecule can be trigonal in shape as evident in Figure 7b, the distance reported here involves only two cluster units and a linker. The sphere diameter was measured to be 1.05 ± 0.13 nm in the dimer and 1.02 ± 0.09 nm in the trimer, which is also consistent with the SAXS fit and the gold core dimensions from the crystal structure reported in literature (0.93 and 0.98 nm respectively).[17] A TEM image of tetramer fraction is shown in Figure 7c, which, consistent with SAXS data, demonstrates that polydispersity of the oligomer increases with its size. Furthermore, it must be emphasised that the distance measured in TEM depends on the projection of the molecule deposited on the grid so it is prone to errors arising from differential oligomer orientation and aggregation.

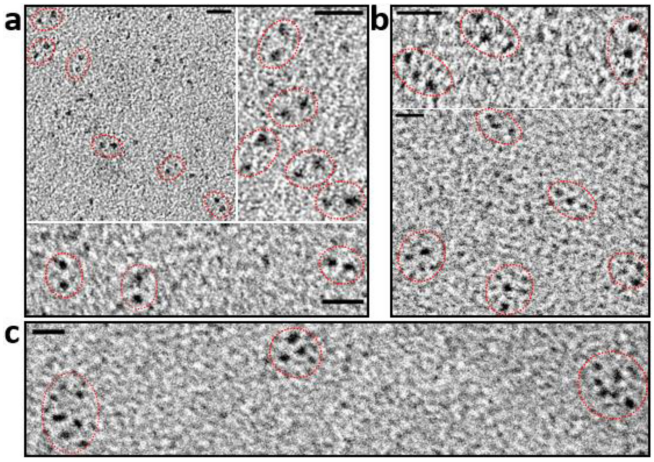

Figure 7. TEM image of isolated (a) dimers, (b) trimers and (c) tetramers imaged at 390kx magnification. The scale bar corresponds to 5 nm. The degree of polydispersity visibly increases with increasing fraction size.

In order to assess the stability of the oligomers formed, a series of unlinking reactions was attempted by mixing the oligomers ($N \approx 2$–3) separately with an excess of PET (200×) and *R*-BINAS (20×). The reaction with the monodentate PET ligand resulted in no difference in absorption spectra after 48 h while the bidentate *R*-BINAS (which, as opposed to PET, should only require an approach of an individual ligand to displace diBINAS) resulted in further flattening of the absorption features (see Figure S12). This is consistent with displacing PET from the clusters rather than unlinking the diBINAS bridge. Further attempts to apply heat to the reaction mixture in order to induce unlinking resulted in the decomposition of the oligomers associated with a large release of free PET ligands, which was not accompanied by a release of free diBINAS (see Figure S13). Overall, the unlinking experiments confirmed that the clusters linked with bidentate diBINAS form very stable systems as any attempts to unlink them were unsuccessful.

Conclusion

The use of diBINAS, a dithiol linker engaging in bidentate bonding, results in a formation of dimers, trimers, tetramers and larger multimers of $Au_{25}PET_{18-2x}$ clusters with high stability and monodispersity owing to the difficulty in breaking of the two Au–S bond simultaneously. The analysis by SAXS was indispensable in confirming the structures of the oligomers and identifying their corresponding UV/Vis spectra. DOSY NMR spectroscopy, DFT calculations, TEM imaging and MALDI-TOF MS elucidated further structural details, while CD measurements demonstrated the emergent properties introduced by the chiral nature of diBINAS. Quantum yield measurements and TCSPC were used to study the fluorescent properties while EPR measurements confirmed the weak nature of the spin-spin coupling in the dimer. Finally, the ineffective unlinking reactions substantiated the high stability associated with the oligomers studied here, laying the foundation for the use of bidentate ligands as templating molecules in the directed self-assembly of metal nanoclusters.

Acknowledgements

Financial support from the University of Geneva and the Swiss National Science Foundation (grant number CRSII5_173720) is kindly acknowledged. This work benefited from the use of the SasView application, originally developed under NSF award DMR-0520547. SasView contains code developed with funding from the European Union's Horizon 2020 research and innovation program under the SINE2020 project, grant agreement No 654000. The help of K. K. Ramankutty with fluorescence measurements is kindly acknowledged. LMLD acknowledges grants from the Swiss National Supercomputing Centre CSCS under project IDs s894 and s1072. Open Access funding provided by Université de Genève.

Conflict of Interest

The authors declare no conflict of interest.

Data Availability Statement

The data that support the findings of this study are openly available in Zenodo at https://doi.org/10.5281/zenodo.7705882.

Keywords: Bidentate · Dimerization · Gold Cluster · Self-Assembly · Small-Angle X-Ray Scattering

[1] a) J. T. Collins, C. Kuppe, D. C. Hooper, C. Sibilia, M. Centini, V. K. Valev, *Adv. Opt. Mater.* **2017**, *5*, 1700182; b) C. Dahmen, G. von Plessen, *Aust. J. Chem.* **2007**, *60*, 447–456; c) C. Gautier, T. Bürgi, *ChemPhysChem* **2009**, *10*, 483–492.

[2] a) W. P. Zhou, A. Lewera, R. Larsen, R. I. Masel, P. S. Bagus, A. Wieckowski, *J. Phys. Chem. B* **2006**, *110*, 13393–13398; b) I. Khan, K. Saeed, I. Khan, *Arab. J. Chem.* **2019**, *12*, 908–931.

[3] a) J.-r. Choi, D.-M. Shin, H. Song, D. Lee, K. Kim, *Nano Convergence* **2016**, *3*, 30; b) M. R. Willner, P. J. Vikesland, *J. Nanobiotechnol.* **2018**, *16*, 95.

[4] Z. He, Z. Zhang, S. Bi, *Mater. Res. Express* **2020**, *7*, 012004.

[5] a) S. Peiris, J. McMurtrie, H.-Y. Zhu, *Catal. Sci. Technol.* **2016**, *6*, 320–338; b) L. Liu, X. Zhang, L. Yang, L. Ren, D. Wang, J. Ye, *Natl. Sci. Rev.* **2017**, *4*, 761–780.

[6] a) R. Awasthi, A. Roseblade, P. M. Hansbro, M. J. Rathbone, K. Dua, M. Bebawy, *Curr. Drug Targets* **2018**, *19*, 1696–1709; b) O. V. Salata, *J. Nanobiotechnol.* **2004**, *2*, 3; c) A. Baghdasaryan, R. Grillo, S. Roy Bhattacharya, M. Sharma, E. Reginato, H. Theraulaz, I. Dolamic, M. Dadras, S. Rudaz, E. Varesio, T. Burgi, *ACS Appl. Nano Mater.* **2018**, *1*, 4258–4267.

[7] a) M. Grzelczak, J. Vermant, E. M. Furst, L. M. Liz-Marzán, *ACS Nano* **2010**, *4*, 3591–3605; b) E. Cara, F. Ferrarese Lupi, M. Fretto, N. De Leo, M. Tortello, R. Gonnelli, K. Sparnacci, L. Boarino, *Nanomaterials* **2020**, *10*, 280.

[8] a) S. Hossain, Y. Imai, Y. Motohashi, Z. Chen, D. Suzuki, T. Suzuki, Y. Kataoka, M. Hirata, T. Ono, W. Kurashige, T. Kawawaki, T. Yamamoto, Y. Negishi, *Mater. Horiz.* **2020**, *7*, 796–803; b) Z. Wu, Q. Yao, S. Zang, J. Xie, *ACS Mater. Lett.* **2019**, *1*, 237–248; c) J.-Y. Kim, J. Yeom, G. Zhao, H. Calcaterra, J. Munn, P. Zhang, N. Kotov, *J. Am. Chem. Soc.* **2019**, *141*, 11739–11744.

[9] a) K. Sokolowska, E. Hulkko, L. Lehtovaara, T. Lahtinen, *J. Phys. Chem. C* **2018**, *122*, 12524–12533; b) A. Sels, G. Salassa, F. Cousin, L.-T. Lee, T. Bürgi, *Nanoscale* **2018**, *10*, 12754–12762; c) T. Lahtinen, E. Hulkko, K. Sokołowska, T.-R. Tero, V. Saarnio, J. Lindgren, M. Pettersson, H. Häkkinen, L. Lehtovaara, *Nanoscale* **2016**, *8*, 18665–18674.

[10] a) P. Chakraborty, A. Nag, B. Mondal, E. Khatun, G. Paramasivam, T. Pradeep, *J. Phys. Chem. C* **2020**, *124*, 14891–14900; b) W. S. Compel, O. A. Wong, X. Chen, C. Yi, R. Geiss, H. Häkkinen, K. L. Knappenberger, C. J. Ackerson, *ACS Nano* **2015**, *9*, 11690–11698.

[11] a) G. Salassa, A. Sels, F. Mancin, T. Bürgi, *ACS Nano* **2017**, *11*, 12609–12614; b) Y. Niihori, S. Hashimoto, Y. Koyama, S. Hossain, W. Kurashige, Y. Negishi, *J. Phys. Chem. C* **2019**, *123*, 13324–13329.

[12] a) S. Knoppe, T. Bürgi, *Phys. Chem. Chem. Phys.* **2013**, *15*, 15816–15820; b) A. Sels, N. Barrabés, S. Knoppe, T. Bürgi, *Nanoscale* **2016**, *8*, 11130–11135; c) Y. Wang, B. Nieto-Ortega, T. Bürgi, *Nat. Commun.* **2020**, *11*, 4562; d) S. Knoppe, A. C. Dharmaratne, E. Schreiner, A. Dass, T. Bürgi, *J. Am. Chem. Soc.* **2010**, *132*, 16783–16789.

[13] a) V. R. Jupally, R. Kota, E. V. Dornshuld, D. L. Mattern, G. S. Tschumper, D.-e. Jiang, A. Dass, *J. Am. Chem. Soc.* **2011**, *133*, 20258–20266; b) C. A. Fields-Zinna, J. F. Parker, R. W. Murray, *J. Am. Chem. Soc.* **2010**, *132*, 17193–17198.

[14] T. Catherall, D. Huskisson, S. McAdams, A. Vijayaraghavan, *J. Mater. Chem. C* **2014**, *2*, 6895–6920.

[15] a) C. M. Aikens, *J. Phys. Chem. Lett.* **2011**, *2*, 99–104; b) M. Zhu, C. M. Aikens, F. J. Hollander, G. C. Schatz, R. Jin, *J. Am. Chem. Soc.* **2008**, *130*, 5883–5885.

[16] a) A. Baksi, A. Mitra, J. S. Mohanty, H. Lee, G. De, T. Pradeep, *J. Phys. Chem. C* **2015**, *119*, 2148–2157; b) T. Li, A. J. Senesi, B. Lee, *Chem. Rev.* **2016**, *116*, 11128–11180.

[17] M. W. Heaven, A. Dass, P. S. White, K. M. Holt, R. W. Murray, *J. Am. Chem. Soc.* **2008**, *130*, 3754–3755.

[18] a) A. Macchioni, G. Ciancaleoni, C. Zuccaccia, D. Zuccaccia, *Chem. Soc. Rev.* **2008**, *37*, 479–489; b) F. Perrin, *J. Phys. Radium* **1934**, *5*, 497–511.

[19] K. Salorinne, T. Lahtinen, J. Koivisto, E. Kalenius, M. Nissinen, M. Pettersson, H. Häkkinen, *Anal. Chem.* **2013**, *85*, 3489–3492.

[20] a) J. Breffke, B. W. Williams, M. Maroncelli, *J. Phys. Chem. B* **2015**, *119*, 9254–9267; b) F. Glöcklhofer, A. Rosspeintner, P. Pasitsuparoad, S. Eder, J. Fröhlich, G. Angulo, E. Vauthey, F. Plasser, *Mol. Syst. Des. Eng.* **2019**, *4*, 951–961.

[21] a) X. Kang, S. Wang, Y. Song, S. Jin, G. Sun, H. Yu, M. Zhu, *Angew. Chem. Int. Ed.* **2016**, *55*, 3611–3614; *Angew. Chem.* **2016**, *128*, 3675–3678; b) R. Kazan, B. Zhang, T. Bürgi, *Dalton Trans.* **2017**, *46*, 7708–7713.

[22] G. Williams, D. C. Watts, *Trans. Faraday Soc.* **1970**, *66*, 80–85.

Manuscript received: October 26, 2022
Accepted manuscript online: February 2, 2023
Version of record online: ■■, ■■

Research Articles

Gold Clusters

M. Swierczewski, F. Cousin, E. Banach, A. Rosspeintner, L. M. Lawson Daku, A. Ziarati, R. Kazan, G. Jeschke, R. Azoulay, L.-T. Lee,* T. Bürgi* _____ **e202215746**

Exceptionally Stable Dimers and Trimers of Au_{25} Clusters Linked with a Bidentate Dithiol: Synthesis, Structure and Chirality Study

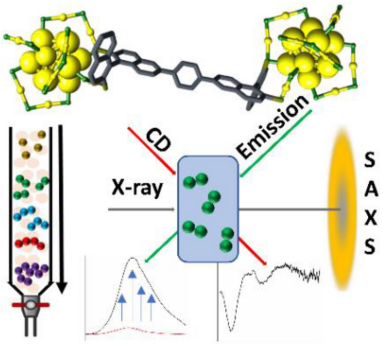

A new chiral dithiol is used to bridge Au_{25} nanoclusters together. Due to its bidentate nature, the dimers and trimers can be isolated before further reaction occurs. The structure of the oligomers is analysed by small-angle X-ray spectroscopy. The changes in optical properties are followed by UV/Vis absorption, fluorescence spectroscopy and circular dichroism.